Empirical Models for NB-IoT Path Loss in an Urban Scenario

Giuseppe Caso, Özgü Alay, Luca De Nardis, Anna Brunstrom, Marco Neri, Maria-Gabriella Di Benedetto

***Abstract*—The lack of publicly available large scale measurements has hindered the derivation of empirical path loss (PL) models for Narrowband Internet of Things (NB-IoT). Therefore, simulation-based investigations currently rely on models conceived for other cellular technologies, which are characterized, however, by different available bandwidth, carrier frequency, and infrastructure deployment, among others. In this paper, we take advantage of data from a large scale measurement campaign in the city of Oslo, Norway, to provide the first empirical characterization of NB-IoT PL in an urban scenario. For the PL average term, we characterize Alpha-Beta-Gamma (ABG) and Close-In (CI) models. By analyzing multiple NB-IoT cells, we propose a statistical PL characterization, i.e., the model parameters are not set to a single, constant value across cells, but are randomly extracted from well-known distributions. Similarly, we define the PL shadowing distribution, correlation over distance, and inter-site correlation. Finally, we give initial insights on outdoor-to-indoor propagation, using measurements up to deep indoor scenarios. The proposed models improve PL estimation accuracy compared to the ones currently adopted in NB-IoT investigations, enabling more realistic simulations of urban scenarios similar to the sites covered by our measurements.**

***Index Terms*—Cellular Internet of Things, massive Machine Type Communications, Narrowband Internet of Things, Path Loss Empirical Models**

I. Introduction

Standardized by 3rd Generation Partnership Project (3GPP) in Release 13 (Rel-13), Narrowband Internet of Things (NB-IoT) is a leading solution in the context of Low Power Wide Area Networks (LPWANs) [1]. It enables low-cost and power-efficient IoT applications by exploiting the cellular infrastructure [2], focusing on massive Machine Type Communication (mMTC) services, such as smart cities, environmental monitoring, and industrial automation, among others [3] [4].

Nowadays, many mobile operators are launching NB-IoT networks worldwide [5], while the research community is addressing several theoretical aspects aiming at deriving solutions for system optimization. As for all wireless technologies, validation of such solutions is often performed via simulations, thus requiring realistic modeling assumptions.

In this context, a key aspect is radio propagation modeling [6], e.g., in terms of path loss (PL) average and variable terms, the latter caused by fading phenomena. Indeed, several research and standardization activities focus on the derivation of realistic PL models for wireless systems. A common solution is the use of so-called empirical models. These consist of parametrized equations, and require real PL measurements for *fitting* such equations, i.e., finding the values of the parameters that minimize the difference between model estimates and real measurements.

The derivation of an empirical model is often challenged by the scarcity of large scale measurement campaigns. As also observed in [7] [8], propagation measurements for cellular systems often assume a single or a few base stations (also, cells). Hence, models usually present fixed values of the parameters (e.g., [9]–[11]). However, the above assumption may be unrealistic in urban scenarios, since it would imply similar PL characteristics for all cells, independent of the environment where cells are deployed (e.g., areas with a majority of high and newer buildings vs. areas with a majority of low and older buildings, areas with high presence of public green vs. areas with low presence of public green, and areas with a majority of wide streets vs. areas with a majority of narrow streets, among others) [12].

First attempts at deriving empirical models have focused on a NB-IoT technology competitor, i.e., Long Range Wide Area Network (LoRaWAN), due to a greater availability of measurements [13]–[15]; LoRaWAN operates, however, in the unlicensed spectrum, and exploits a dedicated infrastructure and specific transmission settings, which limits the application of the obtained models to NB-IoT. As a matter of fact, the lack of publicly available large scale measurements has, so far, hindered the derivation of PL models for NB-IoT. Therefore, in lack of a better option, simulation-based evaluations of NB-IoT have relied on models originally conceived for other cellular technologies, such as Universal Mobile Telecommunications System (UMTS) and Long Term Evolution (LTE) (e.g., [16]–[27], among others). However, peculiar characteristics of NB-IoT when compared with preexisting cellular technologies, e.g., in terms of occupied bandwidth, infrastructure deployment, and operating scenarios (e.g., deep indoor), can be expected to introduce remarkably different propagation characteristics. This observation, confirmed by our results in §V-B, where we compare NB-IoT against LTE, calls for a NB-IoT specific PL assessment and model.

In this paper, we provide the first empirical characterization of NB-IoT PL in an urban scenario. To do so, we exploit a large scale measurement campaign executed in the city of Oslo, Norway, preliminarily analyzed in [28] and made available under an open-source license in [29]. The main contributions can be summarized as follows:

G. Caso is with Simula Metropolitan CDE.
Ö. Alay is with University of Oslo and Simula Metropolitan CDE.
L. De Nardis and M.-G. Di Benedetto are with Sapienza Univ. of Rome.
A. Brunstrom is with Karlstad University.
M. Neri is with Rohde&Schwarz.

We derive the parameters for the PL average term of two empirical models: Alpha-Beta-Gamma (ABG) [30] and Close-In (CI) [30] [31]. Since our measurements include a large amount of NB-IoT cells from two operators, we provide *statistically extended* models, with parameters not fixed to a single value but spanning over distributions, as derived in [12] for other cellular systems;

We analyze the PL fading term based on *shadowing*, and provide statistically extended models for its distribution and correlation over distance, as preliminarily studied in [32] for other cellular systems. Moreover, we provide insights on the inter-site (also, inter-cell) shadowing correlation; given a pair of cells, the shadowing experienced in a common set of measurement points is correlated [7], [8], [33]–[36];

We validate our models across NB-IoT operators, and also against LTE, thanks to the availability of LTE measurements collected in the same campaign. Moreover, we show that the proposed models improve PL estimation accuracy compared to current state of the art, and enable more realistic simulations of propagation in Oslo-like urban areas, while preserving low model complexity;

We exploit a set of (deep) indoor measurements to provide preliminary indications on the additional losses to be considered in NB-IoT outdoor-to-indoor propagation.

The paper is organized as follows. The background is provided in §II, while §III presents experimental design, measurement campaigns, and data processing. The proposed models are derived in §IV, while further discussions and insights are given in §V. Conclusions are provided in §VI.

II. Background

This section provides the background of this investigation. After a short discussion of NB-IoT technology (§II-A), PL modeling solutions commonly adopted for cellular systems are described in §II-B. Literature examples showing how NB-IoT PL modeling are presented in §II-C.

A. NB-IoT technology

NB-IoT is a LPWAN radio interface that leverages the cellular licensed spectrum and architecture [2]–[4]. It operates over either a 200 kHz Global System for Mobile Communications (GSM)-like channel or an LTE Physical Resource Block (PRB) of 180 kHz. It adopts one out of three possible operation modes: a) *stand-alone*, over a 200 kHz channel in the GSM spectrum, b) *in-band*, over a single PRB within a set of LTE PRBs, c) *guard-band*, within a guard band among different sets of LTE PRBs.

After selecting a mode, a mobile operator can provide NB-IoT services via a software upgrade of its infrastructure, i.e., by configuring (some of) its LTE evolved Node Bs (eNBs) with NB-IoT-enabled cells.

In Rel-13, NB-IoT allocates downlink (DL) and uplink (UL) resources using Frequency Division Duplex (FDD), with Time Division Duplex (TDD) introduced in Rel-15. Moreover, Orthogonal Frequency Division Multiple Access (OFDMA) is applied in DL (15 kHz subcarrier spacing), while Single Carrier Frequency Division Multiple Access (SC-FDMA) is used in UL (subcarrier spacing of either 15 kHz or 3.75 kHz).

The definition of DL and UL channels nearly follows LTE, with some simplifications [2]. For this paper, it is worth knowing that, similarly to LTE, NB-IoT cells allocate portions of DL channels to the transmission of the Narrowband Reference Signal (NRS). This allows NB-IoT devices to estimate their propagation conditions in terms of (Narrowband) Reference Signal Received Power (RSRP [dBm]). Based on RSRP and operator's configurations, a device estimates its Coverage Level (CL), which in turn allows to optimize the configurations for performing the Random Access (RA) procedure (i.e., the attachment to a cell) and to exchange data. Depending on the CL, NB-IoT transmissions can be repeated up to 2048 vs. 128 times in DL vs. UL, in order to increase the probability of correct reception in harsh environments (e.g., dense urban and deep indoor). Since NB-IoT targets high service reliability and delay-tolerant data exchange, repetitions are preferred to advanced coding schemes; furthermore, only low order modulation schemes, Quadrature Phase Shift Keying (QPSK) and Binary Phase Shift Keying (BPSK)/QPSK, are adopted in DL/UL.

Finally, in order to ensure high energy efficiency and long battery lifetime, NB-IoT standards introduce two energy saving schemes: the extended Discontinuous Reception (eDRX) and the Power Saving Mode (PSM) [37].

B. PL modeling in cellular systems

We now provide a high-level description of PL modeling solutions commonly used in cellular systems, with particular attention to aspects relevant to NB-IoT, for both outdoor and outdoor-to-indoor propagation.

Outdoor propagation. It is a common practice to represent the PL [dB] on a wireless outdoor link as follows:

$$\mathsf{PL} = \overline{\mathsf{PL}} + X \quad [\mathsf{dB}]; \tag{1}$$

where $\overline{\mathsf{PL}}$ is the average PL and X represents a random variation around the average, that is usually assumed to be caused by slow fading, i.e., shadowing due to obstructing objects.[1]

Different empirical models have been proposed for estimating $\overline{\mathsf{PL}}$ in cellular systems. All are somehow derived from the Free Space (FS) model, which characterizes ideal Line of Sight (LoS) propagation [6].[2] In the FS model, $\overline{\mathsf{PL}}$ is given by:

$$\overline{\mathsf{PL}}_{\mathsf{FS}} = 20\log_{10}(d) + 20\log_{10}(f_c) + 20\log_{10}\left(\frac{4}{c}\right); \tag{2}$$

where d is the Transmitter-Receiver (Tx-Rx) distance (e.g., cell-device distance in a cellular system), f_c is the carrier frequency, and c is the speed of light. Assuming d in km and f_c in MHz, the last term is equal to 32.44 dB.

[1]The effects of fast (also, small scale) fading, mostly due to multipath and mobility, are usually neglected in general PL characterizations, so to remove specific propagation behaviours and local variability [6] [12]. In §III-D, we report the processing steps for removing fast fading from our NB-IoT measurements, while preserving the shadowing component.

[2]The well-known Friis's formula extends FS by considering possible antenna gains at both Transmitter and Receiver sides.

ABG [30] and CI [31] models are widely used, and have also been recently adopted for modeling urban and suburban 5G PL (see [10] [11] [30], among others).

The *ABG model* estimates $\overline{\mathsf{PL}}$ as follows:

$$\overline{\mathsf{PL}}_{\mathsf{ABG}} = 10 \quad \log_{10}(d_{\mathsf{km}}) + 10 \quad \log_{10}(f_{c;\mathsf{MHz}}) + l_0; \qquad (3)$$

where d_{km} is the Tx-Rx distance [km], is a distance-dependent parameter, i.e., the PL exponent, $f_{c;\mathsf{MHz}}$ is the carrier frequency [MHz], is a frequency-related exponent, and l_0 is a constant loss term [dB]. Eq. (3) shows that ABG generalizes the FS model. The name ABG refers to an alternative notation used in literature (see [10] [11], among others), by which variables , , and indicate the PL exponent, constant losses, and f_c-related parameters. In this paper we use instead a more traditional symbolic reference so to have a uniform notation with the CI model.

Similarly, the *CI model* estimates $\overline{\mathsf{PL}}$ as follows:

$$\overline{\mathsf{PL}}_{\mathsf{CI}} = 10 \quad \log_{10} \quad \frac{d_{\mathsf{km}}}{d_0} \quad + \mathsf{A}; \qquad (4)$$

In Eq. (4), d_0 is a reference distance to be defined, while A is either set as the loss at d_0 estimated via FS, or optimized along with in a fitting procedure.

As shown in Eq. (1), the estimated $\overline{\mathsf{PL}}$ is complemented by a sample extracted from a random variable X, modeling the presence of fading. When shadowing prevails, X is commonly assumed to be normally distributed with zero mean ( ) and standard deviation ( ) determined by fitting the $\overline{\mathsf{PL}}$ equation to the available measurements.

In mobile scenarios, an accurate shadowing model should also include its correlation with distance, that is, given a cell, how shadowing experienced at similar distances, in a given cell, is correlated. Gudmundson [32] showed that shadowing autocorrelation can be approximated via a decreasing exponential function over distance, where the decreasing rate depends on environmental factors. Based on [32], 3GPP suggested the following approximation for shadowing autocorrelation in mobile cellular networks [38]:

$$R(\Delta d) = e^{\frac{-|\Delta d|}{d_{\mathsf{cor}}}}; \qquad (5)$$

where $R(\Delta d)$ represents the shadowing autocorrelation at Δd, and Δd is the relative distance between two locations. d_{cor} is the so-called *decorrelation* distance, defined as the distance at which the empirical autocorrelation drops at a value equal to e^{-1}. The problem of how to select d_{cor} is addressed in §IV-C2.

Outdoor-to-Indoor propagation. A practical and quite common solution for modeling this scenario is to add a further term to PL, in order to account for the loss experienced by the signal when penetrating walls, floors, and other obstructing objects, before reaching destination. This additional loss, l_{i} [dB], can be obtained empirically, by observing the extent by which, in average, PL outdoor estimates deviate from real indoor measurements. In Technical Specification (TS) 38.901 [39], 3GPP proposed a distance-based definition for l_{i}, by which $l_{\mathsf{i}} = 0.5 d_{\mathsf{i};\mathsf{m}}$, where $d_{\mathsf{i};\mathsf{m}}$ denotes the indoor component of the cell-device path in meters, from the outer wall to the device.

C. Existing PL models used for NB-IoT

In NB-IoT simulation-based works, several options have been adopted for PL estimation, as summarized in Table I. All investigations reuse models obtained from measurements on other cellular technologies, e.g., UMTS and LTE. As clear from Eqs. (6)-(12) (top next page), such models were defined as extensions of the ABG and CI models, typically embedding cell antenna heights.

TABLE I: Application of PL models to NB-IoT PL estimation.

$\overline{\mathsf{PL}}$ **Formula**	**Literature Examples**	**Fading**	**Indoor Loss** l_{i} [dB]
Eqs. (6)(7)	[16]	Shadowing $N(0; 10)$	20; 30
	[17]–[20]	Flat Rayleigh	20
	[21]	Shadowing $N(0; 8)$	N/A
	[22]	N/A	N/A
	[23]	Flat Rayleigh	10
Eqs. (8)	[24]	N/A	N/A
	[25]	Shadowing $N(0; 9.4)$	10
Eqs. (10)(11)	[26] [27]	Shadowing $N(0; 6)$	10; 20; 30

NB-IoT literature has often relied on the PL model of 3GPP UMTS 30.03 [40], originally proposed for vehicular scenarios in urban and suburban areas, with buildings of nearly uniform height. In this case, $\overline{\mathsf{PL}}$ follows Eq. (6), where $h_{b;\mathsf{m}}$ is the cell antenna height [m].

In 3GPP Technical Report (TR) 45.820 [41], Eq. (6) is rewritten assuming an average cell antenna height of 15 m (i.e., $h_{b;\mathsf{m}} = 15$ m) and $f_{c;\mathsf{MHz}} = 900$ MHz [42], i.e. the carrier frequency of LTE Band 8, also available for NB-IoT deployment [2] [43]. The resulting equation, shown in Eq. (7), has been largely used in NB-IoT simulations (see [16]–[23], among others). A simple recalculation allows its use at $f_{c;\mathsf{MHz}} = 800$ MHz, i.e. the carrier frequency of LTE Band 20, also available for NB-IoT and corresponding to the frequency range adopted by the operators in our measurement campaign (cf. §III).

Other investigations use the Okumura-Hata (OH) model [24] [25]. OH is a traditional model for cellular propagation, valid at frequencies from 150 to 1500 MHz [6]. For urban environments, the model is based on measurements collected in the city of Tokyo, and $\overline{\mathsf{PL}}$ follows Eq. (8). The term C_{OH} depends on the considered urban scenario; for small-to-medium cities, C_{OH} is reported in Eq. (9), where $h_{m;\mathsf{m}}$ denotes the height of the mobile device, usually fixed to a reference value of 1.5 m.

Another option, used for example in [26] [27], is the adoption of 3GPP models for Urban Macrocell (UMa) propagation [38], that estimate PL for LoS and Non LoS (NLoS) separately, as reported in Eqs. (10) and (11). In this case, the cell-device distance is in meters and the carrier frequency is in GHz. Moreover, UMa LoS requires the evaluation of a *break point* distance via Eq. (12), which defines the distance where the LoS

$$\overline{\mathsf{PL}}_{\mathsf{UMTS}} = 40(1 \quad 4 \quad 10 \quad {}^{3}h_{b;\mathsf{m}})\log_{10}(d_{\mathsf{km}}) \quad 18\log_{10}(h_{b;\mathsf{m}}) + 21\log_{10}(f_{c;\mathsf{MHz}}) + 80 \tag{6}$$

$$+$$

$$\overline{\mathsf{PL}}_{\mathsf{TR45:820}} = 37{:}6\log_{10}(d_{\mathsf{km}}) + 120{:}9 \tag{7}$$

$$\overline{\mathsf{PL}}_{\mathsf{OH}} = [(44{:}9 \quad 6{:}55\log_{10}(h_{b;\mathsf{m}})]\log_{10}(d_{\mathsf{km}}) \quad 13{:}82\log_{10}(h_{b;\mathsf{m}}) + 26{:}16\log_{10}(f_{c;\mathsf{MHz}}) + 69{:}55 \quad C_{\mathsf{OH}} \tag{8}$$

$$C_{\mathsf{OH}} = [1{:}1\log_{10}(f_{c;\mathsf{MHz}}) \quad 0{:}7]h_{m;\mathsf{m}} \quad [1{:}56\log_{10}(f_{c;\mathsf{MHz}}) \quad 0{:}8] \quad \text{(for small-to-medium cities)} \tag{9}$$

$$\overline{\mathsf{PL}}_{\mathsf{UMa;LoS}} = \begin{cases} 22\log_{10}(d_{\mathsf{m}}) + 20\log_{10}(f_{c;\mathsf{GHz}}) + 28 & 10 < d_{\mathsf{m}} < d'_{\mathsf{BP}} \\ 40\log_{10}(d_{\mathsf{m}}) + 2\log_{10}(f_{c;\mathsf{GHz}}) + 7{:}8 \quad 18\log_{10}(h'_{b;\mathsf{m}}) \quad 18\log_{10}(h'_{m;\mathsf{m}}) & d'_{\mathsf{BP}} < d_{\mathsf{m}} < 5000 \end{cases} \tag{10}$$

$$\overline{\mathsf{PL}}_{\mathsf{UMa;NLoS}} = 161{:}04 \quad 7{:}1\log_{10}(W_{\mathsf{m}}) + 7{:}1\log_{10}(h_{\mathsf{m}}) \quad \Big| \quad 24{:}37 \quad 3{:}7\left(\frac{h_{\mathsf{m}}}{h_{b;\mathsf{m}}}\right)^{2}\Big|\log_{10}(h_{b;\mathsf{m}})$$
$$+ [43{:}42 \quad 3{:}1\log_{10}(h_{b;\mathsf{m}})][\log_{10}(d_{\mathsf{m}}) \quad 3] + 20\log_{10}(f_{c;\mathsf{GHz}}) \quad [3{:}2(\log_{10}(11{:}75h_{m;\mathsf{m}}))^{2} \quad 4{:}97] \tag{11}$$

$$d'_{\mathsf{BP}} = 4h'_{b;\mathsf{m}}h'_{m;\mathsf{m}}\frac{f_{c;\mathsf{GHz}}}{c}; \qquad h'_{b;\mathsf{m}} = h_{b;\mathsf{m}} \quad 1; \qquad h'_{m;\mathsf{m}} = h_{m;\mathsf{m}} \quad 1 \tag{12}$$

propagation assumes a slightly different behavior. *Effective* antenna and mobile heights are also used, obtained via simple adjustments of the original values, as reported in Eq. (12). For UMa NLoS, two further parameters are needed: street width W_{m} and building height h_{m}, in meters. The applicability range for the parameters is given in [38].

As regards the shadowing term, 3GPP also gives indications on the value to adopt, i.e., 10 dB for UMTS 30.03 [40], 8 dB for TR 45.820 [41], and 4/6 dB for UMa LoS/NLoS [38]. These values are also adopted in NB-IoT simulations (Table I). Observe that some of the works opted for considering fast fading via flat Rayleigh distributions.

For outdoor-to-indoor propagation, a majority of works adopt l_{i} values between 10 dB and 30 dB [41]. These losses represent different indoor conditions, up to deep indoor, that are likely to arise for several NB-IoT use cases (e.g., smart metering). Recent investigations [44]–[46] show that the 3GPP distance-based model for l_{i} fits fairly well NB-IoT measurements above the ground level, while performs poorly below the ground level. Applying this rule is challenging, as it requires precise knowledge of $d_{\mathsf{i;m}}$ and complicates PL estimation.

III. Experimental Design and Data Processing

This section contains our measurement campaign, and provides a description of the adopted measurement system and setup in §III-A, and an overview of the dataset in §III-B. Finally, we show how PL measurements were extracted (§III-C), and data prepared for the subsequent analyses (§III-D).

A. Measurement system

We executed NB-IoT measurements in Oslo using the Rohde&Schwarz (R&S) TSMA6 toolkit, along with an Exelonix device, and a Global Positioning System (GPS) antenna.

R&S TSMA6 is formed by a spectrum scanner and a laptop, where the controlling software, named ROMES4, is installed. It enables passive measurements of 3GPP radio technologies up to 6 GHz, and supports NB-IoT signal decoding in all the operation modes. We also leveraged two further TSMA6 functionalities, i.e., a) *Automatic Channel Detection*, for detecting the technologies in the specified spectrum, and b) *Base Transceiver Station (BTS) Position Estimation*, for estimating the position of the cells.

The Exelonix module is a Qualcomm-based NB-IoT device. We embedded the device with NB-IoT SIM cards of the operators under testing, and connected it to TSMA6 via USB. By doing so, we were able to configure and monitor several device operations, such as cell (re-)selection, CL estimation, and RA, while keeping track of Quality of Service (QoS) of active measurements executed after successful RAs.

The present work exploits passive measurements collected by TSMA6; hence, we do not provide further details on Exelonix device and measurements, for which we refer the interested reader to [47] [48].

B. Measurement campaign and dataset

The measurement campaign covered a period of three weeks in Summer 2019. We enabled the scanner to perform passive measurements on several LTE bands. By doing so, we detected two LTE operators, denoted Op1 and Op2, which also provide NB-IoT in the guard bands of Band 20.

The collection was split into multiple sub-campaigns (simply referred to as *campaigns* in the following), each characterized by different location and time. We conducted several outdoor campaigns while walking or on public transport. We also collected static measurements in indoor and deep indoor environments. The dataset includes morning, afternoon, evening, weekdays, and weekends campaigns.

We performed 22 outdoor campaigns, forming the main data-source for this paper. Due to repeated measurements, some of these campaigns covered the same areas. The same applies to indoor and deep indoor campaigns, containing repeated measurements in a set of unique positions.

Each campaign contains parallel collection of both NB-IoT and LTE coverage measurements, as well as network deployment data for Op1 and Op2. In [29], we provide the list of collected attributes along with the full dataset. Moreover, we also make available a geo-referenced visualization platform for a visual assessment of outdoor measurements and estimated position of Op1 and Op2 eNBs and cells.

In this paper we focus on the RSRP readings from all the cells detected during our campaigns (along with position for cells and measurement points), since this enables the calculation of the experimental PL, used for fitting NB-IoT-specific ABG and CI models.

C. PL derivation from measurements

The evaluation of PL based on NRS from cells is estimated as follows:

$$\mathsf{PL} = P_{\mathsf{tx}}^{\mathsf{NRS}} \quad \mathsf{RSRP}; \tag{13}$$

where $P_{\mathsf{tx}}^{\mathsf{NRS}}$ [dBm] is the power used to transmit NRS.

The decoding of control messages from the cells via TSMA6 allows to retrieve $P_{\mathsf{tx}}^{\mathsf{NRS}}$.[3] For both operators, we observe that cells may use slightly different $P_{\mathsf{tx}}^{\mathsf{NRS}}$ values (in the range of a few dB). Most of cells adopt a value of 29 dBm. Hence, we fix $P_{\mathsf{tx}}^{\mathsf{NRS}} = 29$ dBm for all cells.

In Eq. (13), we assume negligible antenna gains at both device and cell sides. At the device side, this directly follows TMSA6 configurations; at the cell side, we came to this conclusion by observing two experimental facts:

- Differently from LTE, which commonly employs several sectorial cells per eNB, both operators in Oslo have activated a single NB-IoT cell in the majority of their LTE-native eNBs [28], ultimately suggesting that they provide nearly omnidirectional coverage around each cell/eNB for NB-IoT;
- A limited amount of PL readings is already available in the R&S system. Such readings refer to the *serving* cells only, i.e., the cells toward which the Exelonix device has performed RAs [47]. The dataset provided in [48] includes these measurements. Hence, we tested the PL calculation in Eq. (13) against such readings. As shown in Fig. 1, we observe that PL readings nearly follow Eq. (13), ultimately supporting our hypothesis. The observed deviations can be attributed to fading, measurement noise, and different rate and possible mismatch between TSMA6 scanner (which collects RSRP) and Exelonix device (that collects PL of serving cells) acquisitions.

D. Data processing

We execute throughout the paper *per cell* and *operator-agnostic* analyses (apart for §V-A, where we report a comparison between operators). Hence, for each cell in each campaign, the position information provided by BTS Position Estimation and GPS are used to evaluate the distance between cell and measurement points, via the haversine formula [49]. The PL at each distance point is obtained by applying Eq. (13) with the corresponding RSRP value and $P_{\mathsf{tx}}^{\mathsf{NRS}} = 29$ dBm.

[3]This parameter is named `nrs_Power_r13` and is shared along with other parameters in the so-called System Information Block 2 (SIB2) messages.

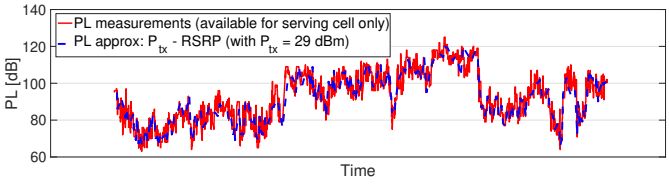

Fig. 1: A comparison of PL readings available in the R&S system vs. PL evaluation in Eq. (13). PL readings are only available for cells toward which the NB-IoT device has performed RAs. Eq. (13) allows to extend the pool of cells under study, including the ones for which the scanner has information on $P_{\mathsf{tx}}^{\mathsf{NRS}}$ and RSRP.

Since outdoor measurements have been collected under medium-to-high mobility, a filtering is needed in order to remove fast fading. To do so, we follow the so-called 40 *-rule* proposed in [50], i.e., we apply a moving average window to the set of PL measurements for each cell. After filtering, each PL value is the average of measurements in a range of 20 (i.e., 37.5 cm @ 800 MHz) from its location.

In order to account for positioning errors due to BTS Position Estimation and GPS inaccuracies (in the range of tens of meters), we fix a distance $d_0 = 0.05$ km and discard, for each cell, all the measurements with $d < d_0$. This value is also used as CI reference distance.

In each campaign, a large number of cells is usually detected. Some of the cells may be represented by a low number of data points, which does not allow for accurate PL characterizations, particularly when such points are at large distances from cells, due to model unreliability. In order to consider this effect, while preserving a large enough amount of cells and treating each campaign equally, we select the 30 top cells for each campaign, i.e., the 30 cells having the largest number of data points. Then, we discard from this pool the cells having the nearest data point at a distance greater than 1 km. This results in a rather symmetric distribution of discarded cells across campaigns, with a median of 5 cells discarded. The campaigns covering smaller (larger) areas (i.e., walking and driving campaigns) have a lower (higher) number of cells discarded. The extreme cases are of 2 and 16 discarded cells for a walking and a driving campaign.

Finally, we observe that, being in urban scenarios, it is likely that the campaigns include both LoS and NLoS measurement points. A classification per point is rather difficult due to the large number of cells and measurements. Hence, we follow the approach in [12], adopted in several empirical models, and analyze the measurements without separating LoS/NLoS points. Indeed, as discussed in §IV, we aim at providing models for mixed LoS/NLoS urban situations, which is key for NB-IoT simulations.

IV. ABG and CI Models for NB-IoT

In this section, we present the steps leading to the NB-IoT PL models proposed in this paper. After assessing the accuracy of existing models (§IV-A), we characterize the main terms of Eq. (1). Hence, we first fit ABG and CI equations for $\overline{\mathsf{PL}}$ estimation (§IV-B), and then focus on the shadowing

term (§IV-C). For the latter, we also discuss the autocorrelation with respect to Eq. (5). A summary of obtained results is given in §IV-D, where we also highlight the main use cases of the proposed models.

A. Comparison of existing models

First, we analyze how the models currently used in NB-IoT simulations perform in terms of PL estimation accuracy against the values in our outdoor campaigns in Oslo. Besides the models in Eqs. (6)–(11), we also report, here and in the next sections, the performance obtained by the FS model, in order to quantify the deviations between ideal and observed propagation characteristics, and better highlight how such deviations are handled by existing and newly proposed models.

Given each campaign, we use the existing models for estimating $\overline{\mathsf{PL}}$ for each cell and corresponding distances. Then, we evaluate the Root Mean Square Error (RMSE) on the differences between PL measurements and $\overline{\mathsf{PL}}$ estimates.

As expressed in Eqs.(6)–(11), some of the models require environment configurations, such as, $h_{b;\mathsf{m}}$, $h_{m;\mathsf{m}}$, h_{m}, and W_{m}. Our campaigns are *in the wild*, i.e., on operational networks. Hence, retrieving information on the above values (e.g., the height of each detected cell) is rather challenging. Under this uncertainty, a widespread option is to simulate PL propagation by using reasonable average values for the above parameters. Hence, cell height $h_{b;\mathsf{m}}$ was fixed to 15 m, the mobile device height ($h_{m;\mathsf{m}}$) to 1.5 m and, for UMA NLoS, the building height and street width (h_{m} and W_{m}) to 25 m and 12 m, respectively.

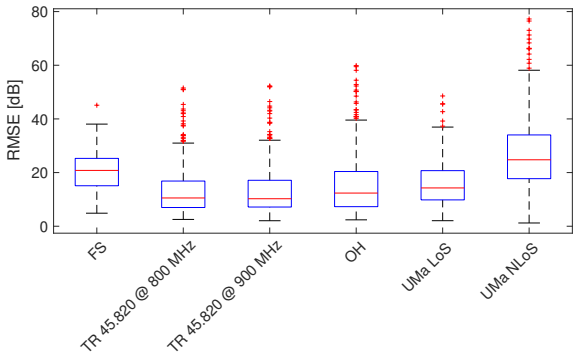

Fig. 2: Comparison of existing PL models adopted in NB-IoT literature. For each model, RMSE statistics across cells are reported.

Fig. 2 shows the statistics of RMSE for each model across cells. All models have rather high RMSE values, that highlight poor PL estimation accuracy. This is due to several reasons, including the fact that the values adopted in such models are not fitted on NB-IoT measurements, and hence they fail to accurately represent propagation behaviour. Furthermore, the need for fixing the environmental variables might also negatively affect the accuracy of some of the models. However, as anticipated above, this is a common procedure in simulation-based studies, where the assumption of perfect knowledge of such configurations is rarely met.

Note that TR 45.820 minimizes the median RMSE to about 10 dB, thus proving to be a reasonable option in absence of a NB-IoT specific model. OH and UMa LoS slightly increase the RMSE compared to TR 45.820, while UMa NLoS and FS bring the median RMSE up to 20 dB, showing that they may significantly overestimate (or underestimate for FS) $\overline{\mathsf{PL}}$, due to the assumption of full NLoS (or ideal for FS) propagation, which is likely not representative of urban scenarios where mixed LoS/NLoS situations naturally arise.

B. $\overline{\mathsf{PL}}$ characterization

In this section, we characterize NB-IoT $\overline{\mathsf{PL}}$ for both ABG and CI models. Throughout §IV-B1 and §IV-B2, we analyze the propagation characteristics across multiple cells in order to a) obtain statistically extended models, i.e., distributions from which some of the model parameters can be selected, while b) keeping the models simple, by fixing some of the other parameters.

1) Unconstrained fitting: We now derive NB-IoT specific parameters for ABG and CI models, i.e., values and distributions of , , and l_0 for ABG, and and A for CI. In this phase, we execute dedicated least squares procedures for each cell, by adopting *unconstrained fitting*, i.e., no constraints on the search spaces of the parameters were used.

Fig. 3 reports the results of the least squares procedure on a reference cell.

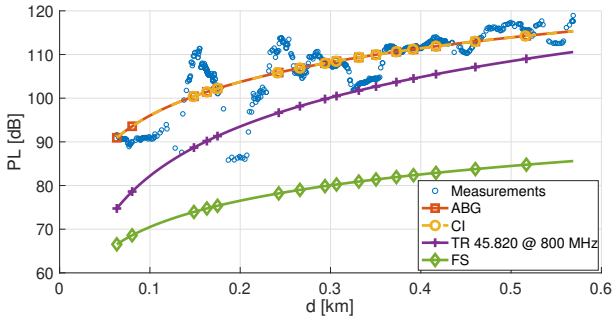

Fig. 3: An example of unconstrained fitting results on a reference cell. ABG and CI estimates are compared against real measurements. FS and TR 45.820 estimates are reported for comparison.

We observe that ABG and CI tend to converge to similar estimate for $\overline{\mathsf{PL}}$ and both follow the measurement trend, apart for expected deviations due to shadowing. For comparison, Fig. 3 also includes FS and TR 45.820 models, and shows that both models lead to an underestimation of $\overline{\mathsf{PL}}$ compared to real measurements. For this cell, the fitting leads to the parameters of Table II. Both models have the same value for ; then, the value for A in CI groups the contributions from and l_0 in ABG.

TABLE II: Values of ABG and CI parameters obtained with unconstrained fitting on a reference cell.

Model			l_0 or A
ABG	2.56	2.97	35.27
CI	2.56	–	88.30

Note that the two models tend to converge to similar parameters for a large number of cells, ultimately suggesting

that a two-parameters model, such as CI, may be accurate enough for estimating $\overline{\mathsf{PL}}$. The variance of values of is, however, high across cells, confirming that, as discussed in §I, cells deployed in an urban area result in significantly different propagation behaviours, due to the heterogeneity of the surrounding environment. In addition, the corresponding distributions do not converge to well-known shapes. An analysis of both models was carried out, aiming at a better simplicity vs. accuracy tradeoff, by focusing on the values of l_0 and A. Fig. 4 reports the empirical probability density function (PDF) for fitted l_0 and A values across cells.

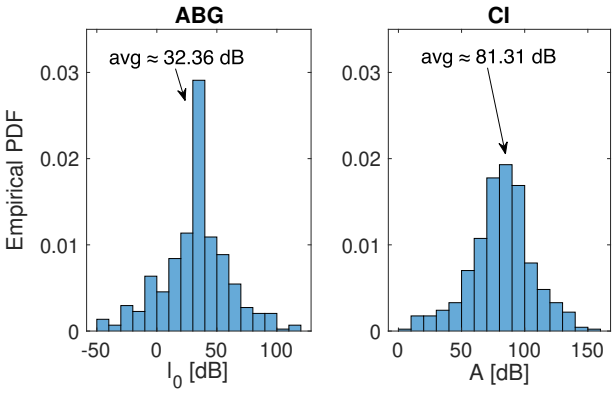

Fig. 4: Empirical PDFs and averages for fitted values of l_0 (left) and A (right), obtained across cells with unconstrained fitting.

We observe that both distributions are nearly symmetric, and values close to the averages occur frequently. This is particularly evident for ABG (left chart of Fig. 4), where the average l_0 value is 32.36 dB. Note that the average value is very close to the value of l_0 in the FS model (32.44 dB, see §II-B), as also obtained in [12].

As for CI, the fitted values of A (right chart of Fig. 4) also concentrate around the average value (81.31 dB). However, this latter significantly diverges from the loss estimated by applying FS at d_0, that is the value at which A should be fixed when not obtained from fitting (cf. §II-B). In our case, this value would correspond to about 64.48 dB, given $f_c = 800$ MHz and $d_0 = 0.05$ km.

In order to simplify the models and stabilize the fitting, we fix l_0 to the FS term (32.44 dB) for ABG, and A to the value derived empirically for CI (81.31 dB) [12]. In the next section, we show the impact of fixing such terms on model accuracy, and also quantify the effect of fixing A to the value *suggested* by FS (64.48 dB).

2) Constrained fitting: The least squares procedure was applied to both models, after fixing l_0 and A values, and the values obtained for the other parameters across cells were analyzed. Fig. 5 (top next page) shows the PDF of the values obtained for and for ABG with $l_0 = 32.44$ dB (Figs. 5a and 5b), and for for CI with $\mathsf{A} = 81.31$ dB (Fig. 5c). Differently from the unconstrained case, the parameters seem to follow normal distributions. The normality was verified at 5% significance level via the Lilliefors test [51]. Fig. 5 also reports the means and standard deviations of the normal distributions better representing the measurements. The values for are normally distributed also for CI with $\mathsf{A} = 64.48$ dB (not in Fig. 5 for space limitations).

Focusing on the distributions for , observe that the averages are about 2.4 (CI) and 2.8 (ABG), which are reasonable values compared to previous studies on urban propagation @ 800-900 MHz (e.g., [52] for LoRaWAN).

Note that distributions also include negative values. Previous investigations also report negative or near-zero values in urban scenarios. In particular, in [8] [9] it is observed this range of values could be obtained a) when measurement points span over too short distance ranges, and b) because buildings may shadow the cell signal at short distances, with this effect reducing with increasing distance, when buildings may tend to disappear from the cell-device path. Our case shows that negative values also appear in the unconstrained fitting case and are thus not caused by the choice of fixing some of the parameters. Moreover, no significant difference between path lengths leading to negative vs. positive values is observed. In conclusion, this result intrinsically shows the complex nature of urban propagation, where several environmental features (e.g., multiple high buildings) may lead to conditions that depart from *nominal* propagation characteristics.

The proposed models embed the above realistic propagation patterns, leading to rather high variability in the considered scenarios. Hence, when applied to simulation-based studies, we suggest to perform a reasonable amount of repeated tests, so to consider a sufficient number of scenarios and provide reliable average performance.

As a further analysis, we quantify a) the accuracy loss of fixing l_0 and A in ABG and CI, compared to the unconstrained cases, and b) the accuracy gain of ABG and CI (with fixed terms) compared to PL models adopted in NB-IoT literature. In order to do so, we define G_{RMSE} as the RMSE loss (resp. gain) obtained by adopting one model vs. another. Given a model, we evaluate RMSE for each cell; then, we average across cells, obtaining $\overline{\mathsf{RMSE}}$. Finally, considering two models, we evaluate the ratio of their $\overline{\mathsf{RMSE}}$ values, which in turn defines G_{RMSE}. By definition, $G_{\mathsf{RMSE}} > 1$ represents an accuracy loss in adopting the model at the numerator of G_{RMSE} and, conversely, an accuracy gain for the model at the denominator of G_{RMSE}, since it indicates a lower $\overline{\mathsf{RMSE}}$ for the latter.

First, we study G_{RMSE} as the ratio between ABG and CI with fixed l_0 and A (at the numerator) and corresponding ABG and CI with unconstrained fitting (at the denominator). As regards ABG, we obtain $G_{\mathsf{RMSE}} = 1$, meaning that fixing l_0 does not cause any accuracy loss compared to the unconstrained case. This is explained by observing that constrained fitting achieves in all cases the same minima of the unconstrained counterpart, thanks to the possibility of adjusting and values when l_0 is fixed. For CI, we obtain instead G_{RMSE} 1.5 with $\mathsf{A} = 81.31$ dB, and G_{RMSE} 1.9 with $\mathsf{A} = 64.48$ dB. Hence, oppositely to ABG, CI is negatively affected by fixing A, since this leads to local minima during the fitting procedure and, in turn, accuracy losses. $\mathsf{A} = 64.48$ dB results in the highest loss and, therefore, it is not investigated further.

Fig. 6 shows G_{RMSE} as the ratio between existing models (at the numerator) and ABG and CI with fixed l_0 and A (at

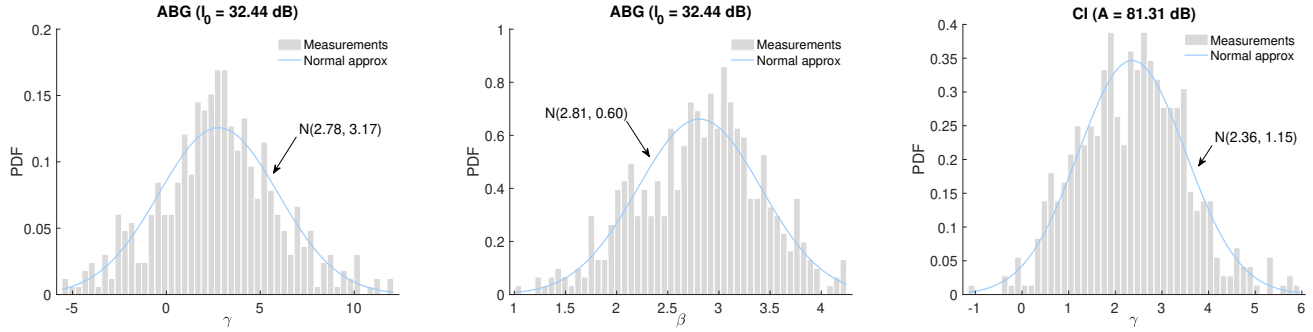

(a) (b) (c)

Fig. 5: Empirical PDFs for fitted values of and (left and middle) for ABG, and for CI (right), obtained across cells with constrained fitting. The nearest normal approximations and corresponding parameters are also reported.

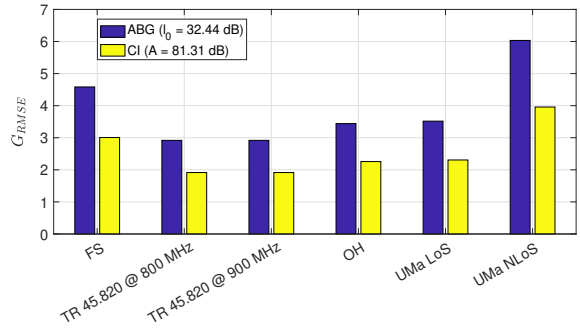

Fig. 6: Proposed vs. existing models: G_{RMSE} represents the gain in terms of $\overline{\mathsf{RMSE}}$ (across cells) of using ABG and CI models with fixed l_0 and A compared to existing models.

TABLE III: Values of and for the nearest normal distribution approximating $\mathcal{X}$. Values are evaluated for ABG and CI with unconstrained fitting on a reference cell. FS and TR 45.820 approximations are reported for comparison.

Model		
ABG	0	4.04
CI	0	4.04
TR 45.820 @800 MHz	8.76	4.93
FS	28	4.25

the denominator). We observe significant gains of both fitted models with respect to existing ones. Since ABG provides higher gains compared to CI, we suggest this model as the primary modeling option; however, in the next sections, we still report results obtained by CI, since this provides a reasonable modeling option and a good benchmark for ABG.

C. X characterization

After analyzing $\overline{\mathsf{PL}}$, we provide insights on the error obtained by comparing PL measurements and $\overline{\mathsf{PL}}$ estimates. This quantifies the accuracy of $\overline{\mathsf{PL}}$ models, and provides insights on shadowing distribution (§IV-C1) and correlation over distance (§IV-C2).

1) Distribution: As explained in §II-B, models with good accuracy result in zero-mean normally distributed shadowing (in dB), that is, X $N(\ = 0;\ )$, where is the distribution mean and is the standard deviation.

In both unconstrained and constrained fitting cases, the differences between ABG and CI estimates and measurements nearly follow normal distributions for most of the cells, in particular when these are represented by a large enough number of measurements.

Table III reports the values of and of the normal distribution better approximating the empirical X for the cell taken as reference in previous sections.

As expected, ABG and CI converge to a same zero-mean normal distribution. As a comparison, the results obtained for FS and TR 45.820 show that, due to $\overline{\mathsf{PL}}$ underestimation, the convergence to a zero-mean distribution is not achieved. Note that existing models may also overestimate $\overline{\mathsf{PL}}$. For example, considering the same cell, we report a negative value of for OH ($=$ 0.91) and UMa NLoS ($=$ 15.54).

In order to analyze this aspect further, we report in Fig. 7 (top next page) the empirical distribution of the means of the normal distributions better approximating X across cells. For both ABG and CI, we see how typical values for approach zero. The deviation from zero increases for CI, due to the fact that it leads to slight accuracy decreases. We also see that TR 45.820 roughly preserves a zero average, but the deviations are quite significant, with values for spanning in a range exceeding 20 dB. This suggests that such a model alternatively underestimates and overestimates $\overline{\mathsf{PL}}$, providing quite unstable estimates compared to real measurements. Finally, FS constantly underestimates $\overline{\mathsf{PL}}$, resulting in a high average value of (about 19 dB). Overall, the analysis leads to the conclusion that fitted ABG and CI provide zero-mean normally distributed shadowing, contrarily to other models.

We now observe how values distribute across cells.

Fig. 8 (top next page) shows that for both ABG (Fig. 8a) and CI (Fig. 8b), follows left-skewed distributions. By means of the Akaike Information Criterion (AIC), we find that Generalized Extreme Value (GEV), Nakagami, and Weibull distributions can approximate well the measured values, since they minimize AIC compared to other distributions. Figs. 8a and 8b report GEV, Nakagami, and Weibull distributions better approximating the empirical PDFs for both models. We report in Table IV the parameters for GEV and Weibull approximation. Due to practicality, we suggest Weibull as the approximation for in both models.

The obtained result differs from [12], which suggested a normal distribution for ($\overline{\mathsf{PL}}$ is estimated via CI with fixed A). The difference might depend on several factors, i.e., different technologies (traditional cellular vs. NB-IoT),

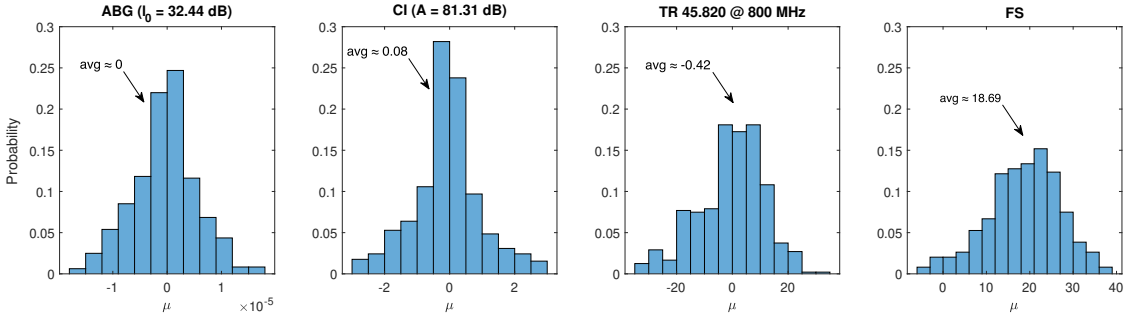

Fig. 7: Empirical PDFs and averages of the values of shadowing expected value , obtained across cells with constrained fitting for ABG (left) and CI (middle left). Distribution and average for TR 45.820 (middle right) and FS (right) are reported for comparison.

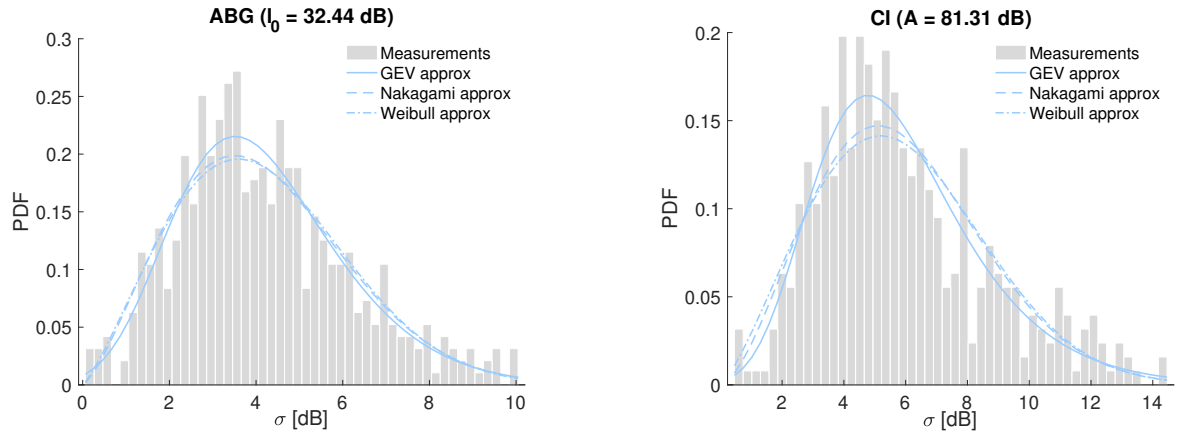

(a) (b)

Fig. 8: Empirical PDFs for fitted values of for ABG (left) and CI (right), obtained across cells with constrained fitting. The nearest GEV, Nakagami, and Weibull approximations are also reported.

TABLE IV: Parameters for GEV and Weibull distributions better approximating the empirical distribution of values. We suggest Weibull approximation (bolded) due to simplicity.

Model	GEV			Weibull	
	Location	Shape	Scale	**Shape**	**Scale**
ABG	3:337	0:102	1:717	2:218	4:709
CI	4:684	0:041	2:240	2:289	6:670

frequencies (1:9 GHz vs. 800 MHz), and scenarios (suburban vs. urban). A Weibull approximation leads to the following while simulating shadowing in a multi-cell urban scenario, the models allow for a zero-mean normal approximation, with of different cells extracted from a Weibull distribution.

2) Autocorrelation: After discussing the distribution, we characterize NB-IoT shadowing correlation and embed this aspect in the proposed models, also for better representing propagation in mobile conditions.

First, we take the shadowing terms over distance and evaluate d_{cor} for each cell, as defined in Eq. (5). Fig. 9 (top next page) depicts the empirical distribution of d_{cor} values for ABG (Fig. 9a) and CI (Fig. 9b). Similarly to , d_{cor} also follows left-skewed distributions; by means of the AIC, we find that Gamma and Weibull distributions can approximate well the empirical PDFs, as also shown in Fig. 9. The distribution parameters are reported in Table V. Aiming at model simplicity, we suggest the adoption of Weibull approximation.

TABLE V: Parameters for Gamma and Weibull distributions better approximating the empirical distribution for the values of d_{cor} [m]. We suggest Weibull approximation (bolded) due to simplicity.

Model	Gamma		Weibull	
	Shape	Scale	**Shape**	**Scale**
ABG	1:234	10:92	1:134	14:11
CI	1:339	19:97	1:197	28:45

For both models, d_{cor} typical values are rather low (i.e., less than 10-20 m in most cases), suggesting that, as the distance to a cell surpasses d_{cor}, the shadowing correlation tends to vanish and be negligible, as modeled by the 3GPP approximation in Eq. (5). We exemplify this observation for a reference cell in Fig. 10, that shows the shadowing autocorrelation as a function of distance, with shadowing terms resulting from the adoption of ABG and CI models to our measurements.

For this cell, d_{cor} is about 10 vs. 20 m for ABG vs. CI. Therefore, we embed such values in Eq. (5) and also report the corresponding approximations in Fig. 10.

The exponential function proposed by 3GPP is quite accurate in approximating shadowing autocorrelation up to d_{cor}. Then, at larger distances, the empirical trends tend to deviate from the approximation in a random manner. Indeed, the observed rises and falls are due to random situations not accounted for in the model. Since this behaviour is observed across cells, we conclude that, on average, NB-IoT shadowing correlation indeed vanishes over distance. Therefore, it can be safely modeled by Eq. (5), using d_{cor} values sampled from the distributions of Fig. 9.

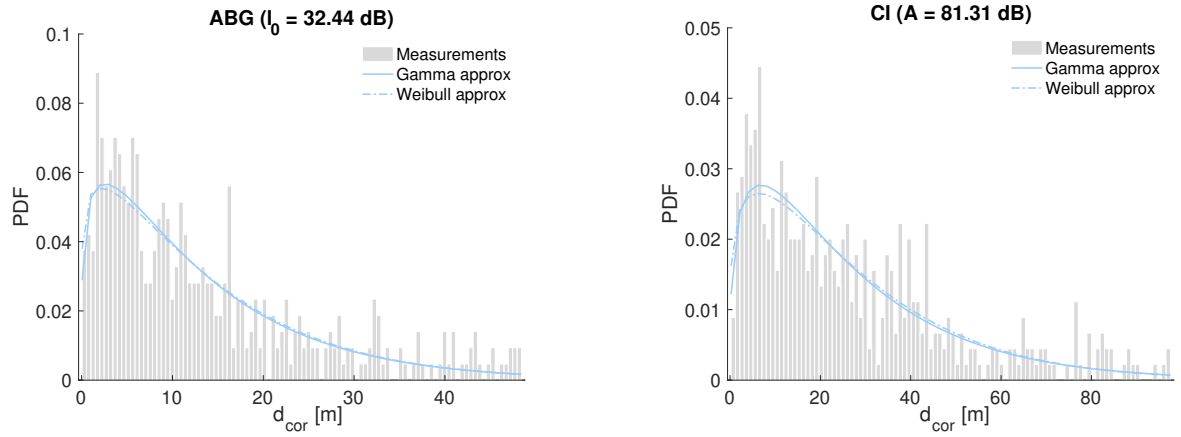

(a) (b)

Fig. 9: Empirical PDFs for the values of d_{cor} [m] for ABG (left) and CI (right), obtained across cells with constrained fitting. The nearest Gamma and Weibull approximations are also reported.

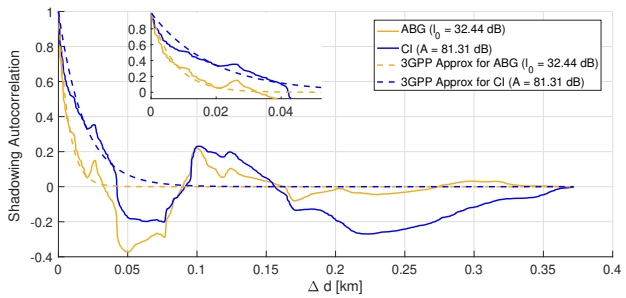

Fig. 10: An example of shadowing autocorrelation on a reference cell. The empirical autocorrelation for ABG and CI models (with constrained fitting) is compared against corresponding 3GPP approximations after the evaluation of d_{cor} (Eq. (5)).

D. Model Summary and Usage

Table VI summarizes the main results derived in §IV. We assume the use of ABG or CI models for simulating NB-IoT propagation from multiple cells deployed in an urban area similar to the city of Oslo, i.e., a medium size outdoor environment with buildings of different heights and mostly wide streets. For $\overline{\text{PL}}$, the models have fixed values for l_0 and A terms. Then, they allow to associate different parameters to each cell, in terms of and (ABG), and (CI). Such values are extracted from normal distributions.

The shadowing term is zero-mean normally distributed with cell-dependent standard deviation . For both models, the values for are extracted from Weibull distributions. Assuming a simplistic modeling, the shadowing terms at each distance from a cell can be independently generated; for more realistic modeling, also including mobility scenarios, their correlation over distance should be modeled via Eq. (5), with the value of d_{cor} for each cell extracted from a Weibull distribution.[4] The parameters for all the distributions are reported in Table VI.

V. Model Evaluation and Further Discussions

In this section, we perform further analyses, in order to evaluate the proposed models. First, we perform a comparison between NB-IoT operators in §V-A, thus assessing the differences between them and how the proposed operator-agnostic models can be used for estimating corresponding $\overline{\text{PL}}$. Then, we propose a technology comparison with LTE (§V-B), and show that NB-IoT and LTE present significant differences in their propagation characteristics, even though working at the same frequencies and exploiting similar infrastructure, ultimately justifying the adoption of a dedicated PL model for NB-IoT. In terms of shadowing, we discuss inter-site correlation in §V-C, while in §V-D we analyze NB-IoT indoor measurements, providing initial insights for using the models in outdoor-to-indoor scenarios.

[4]See [40, Annex D, §4] for further details on how to use the shadowing autocorrelation function in PL models.

TABLE VI: Summary of proposed ABG and CI parametrization for NB-IoT PL modeling in urban scenarios.

Parameter	**ABG** [Eq. (3)]	**CI** [Eq. (4)]
	N (2:78; 3:17)	N (2:36; 1:15)
	N (2:81; 0:60)	–
l_0 or A [dB]	32:44	81:31
X	N (0;)	N (0;)
[dB]	Wbl(4:709; 2:218) [(a)]	Wbl(6:670; 2:289)
Shadowing autocorr.	Eq. (5)	
d_{cor} [m]	Wbl(14:11; 1:134)	Wbl(28:45; 1:197)

[(a)] Wbl(x; y) stands for Weibull distribution with scale x and shape y.

A. Comparison across operators

We analyze how the operator-agnostic $\overline{\text{PL}}$ models map over operator-specific PL characteristics and infrastructures.

We perform unconstrained and constrained fitting after splitting the cells across Op1 and Op2. As a result of unconstrained fitting, we observe that, for both operators, the distributions of l_0 and A are still symmetric. Op1 has an average value of 32:01 dB for l_0 and 79:38 dB for A, while the values for Op2 are 33:12 dB and 82:95 dB. Compared to operator-agnostic approximation, we see small deviations that justify the use for both operators of the average values obtained in the previous section. We also notice that Op1 has smaller losses compared to Op2, which could be an effect of its denser and better deployment, including a larger number of better located NB-IoT cells compared to Op2 [28].

We thus fix again l_0 to 32:44 dB and A to 81.31 dB, and perform constrained fitting across the operators' cells. Figure 11 shows the normal distributions better approximating the

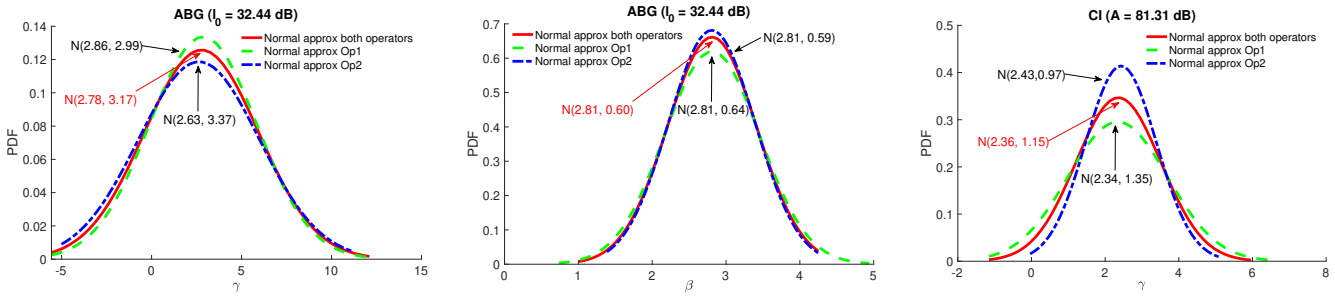

(a) (b) (c)

Fig. 11: Comparison between NB-IoT operators in terms of distribution of the values of and (left and middle) for ABG, and for CI (right), across cells with constrained fitting. The nearest normal approximations and corresponding parameters are reported for both operators, and the global normal approximation is shown for comparison.

empirical PDFs obtained for (ABG and CI) and (ABG). We show normal approximations since, also in this case, most of the distributions pass the normality test. As shown in Fig. 11, operator-specific slightly deviate from operator-agnostic distributions. Indeed, the latter are essentially the averages of the former, apart for numerical approximations due to outliers' removal, which we perform on all the distributions in order to rule out the inaccuracies of some collected measurements. Overall, the results verify that the proposed models provide reliable estimates across different operators and infrastructures.

B. Comparison with LTE

We perform a comparison with LTE in order to further highlight the need for a NB-IoT specific PL model.

As mentioned in §III-B, our campaigns include parallel NB-IoT and LTE coverage measurements. We have already assessed in [28] that NB-IoT deployment choices for Op1 and Op2 are a substantial reuse of their LTE infrastructures. Moreover, in most cases, the operators exploit multiple LTE sectorial cells per eNB and at different frequencies while, at the time of our measurements, a single NB-IoT cell per eNB was mostly used in the guard bands of LTE Band 20. Therefore, the dataset allows a comparison of NB-IoT and LTE propagation in a large urban area. For LTE, we focus on Band 20 and perform the same analyses carried out for NB-IoT. Due to sectorial deployment, an antenna gain is added in Eq. (13). We use a common value adopted in LTE link budget analyses, i.e., 17 dBi [38].

First, we report that LTE results in a significantly lower number of measurement points, i.e., measurement locations, per cell, with a median value decreasing from 200 for NB-IoT to less than 100. This finding already highlights that NB-IoT propagation is intrinsically different than LTE. Most likely due to the fact that the transmitted power is focused on a smaller band, NB-IoT signals are more penetrating than LTE ones, and thus require specific analyses for better PL characterization.

Figure 12 shows how l_0 and A values distribute when unconstrained fitting is performed for LTE cells. Similarly to NB-IoT, the values distribute symmetrically, but have significantly higher averages, i.e., about 46 dB and 110 dB for l_0 and A, respectively. Essentially, this confirms that, in the same environment and exploiting the same infrastructure, LTE experiences higher losses compared to NB-IoT.

Once fixed l_0 and A to the average values, we execute constrained fitting and find that and nearly follow normal distributions also for LTE, although the normality hypothesis is rejected by the Lilliefors test, probably due to instability caused by smaller datasets. LTE has an average of 2.33 (ABG) and 1.78 (CI), and an average of 3.14. Higher variances are also observed compared to NB-IoT in all cases.

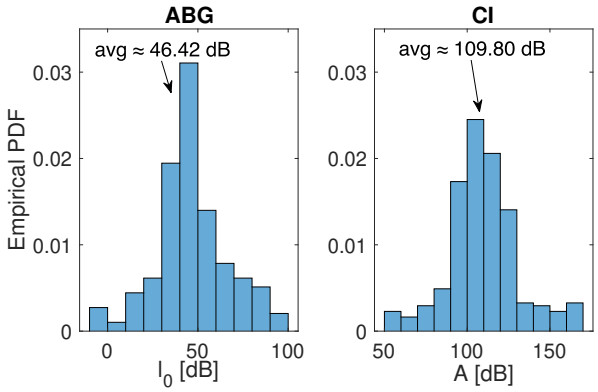

Fig. 12: Empirical PDFs and averages for fitted values of l_0 (left) and A (right), obtained across LTE cells with unconstrained fitting.

C. Inter-site correlation

As a further analysis related to shadowing, we study inter-site (shadowing) correlation. We observe that this aspect is usually not embedded in PL models; hence, we also do not aim at this for the proposed models. However, its investigation allows to shed light on the complexities of urban propagation, and is beneficial for network planning and optimization, e.g., for deriving solutions for improving coverage and co-channel interference management.

Inter-site correlation has been studied and demonstrated in several works addressing PL analysis via measurements from multiple cells [7], [8], [33]–[36]. In our analysis, we follow the approach of previous works and study this aspect by considering three main factors, i.e., given a pair of cells, a) the distance between each cell and the set of measurement locations common to both, b) the distance between cells, and c) the angle between cells. Then, the inter-site correlation is evaluated on the shadowing terms measured in the common measurement locations.

Given a pair of cells, the distance between each cell and the set of common measurement locations is approximated to

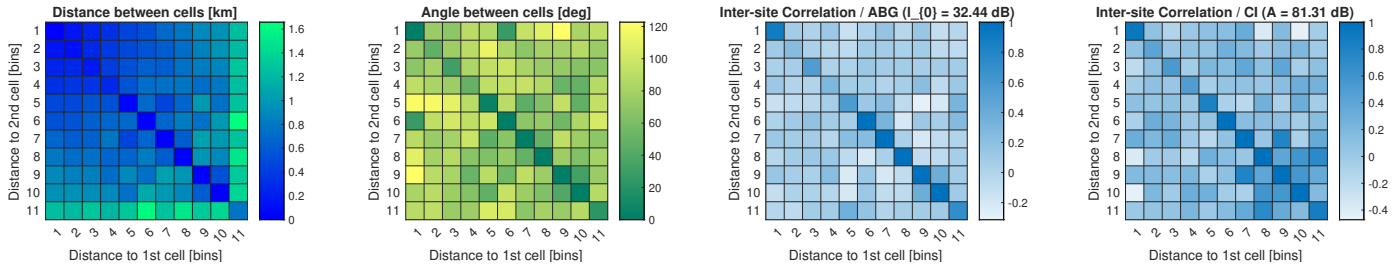

Fig. 13: Distance (left), angle (middle left), and inter-site shadowing correlation (ABG: middle right, CI: right) between pairs of cells, as a function of the distance between each cell and the set of common measurement locations. Heatmaps show median values for each indicator, evaluated across the pairs of cells in any bin.

the distance between each cell and the middle location of such common set. The middle location is identified by alternatively ordering the full set of common locations with respect to the distance from one cell or the other. Since many different distances can be actually observed, we simplify the analysis by quantizing this indicator, i.e., by grouping distances in bins. As shown in Fig. 13, we use eleven bins. The distance to a cell, d_{cell} [m], belongs to bin $x = 1$ if $0 < d_{\text{cell}}$ 100 m (i.e., the cell is less than 100 m away from the set of measurements), while it belongs to bin $x = 11$ if $d_{\text{cell}} > 1000$ m (i.e., the cell is more than 1 km away from the set of measurements). d_{cell} belongs to bin x 2 $[2; 10]$ if $(x \quad 1) \quad 100 < d_{\text{cell}} \quad x \quad 100$ m.

In Fig. 13, the first two heatmaps show distance and angle between cells as a function of d_{cell}. These would help to interpret the next two heatmaps, that show the inter-site correlation for ABG and CI, respectively. Given a joint bin in each heatmap (e.g., bin 1-1, that shows situations where, given a pair of cells and their common measurement locations, d_{cell} 100 m for both cells), the heatmaps show the median values of the other variables, evaluated over all the pairs of cells belonging to that bin.

The heatmaps show a peculiar behaviour at the diagonal. We observe that when the distances between the cells and the common measurements are equivalent (i.e., we are on the diagonal), distances and angles between cells are minimized. This suggests that, in our campaigns, we often observe situations where two cells are *near* each other, and they are jointly detected in a common set of measurement points. In such situations, we see from the last two heatmaps that the inter-site correlation is maximized, even when the collected measurements are far away from both cells (e.g., bin 10-10 or bin 11-11). This confirms previous results in [33]–[35], which demonstrated the inverse relationship between angle and inter-site correlation between two cells. Outside the diagonal, the pattern is more confused, and does not allow to highlight a general behaviour.

Overall, results show the presence of inter-site shadowing correlation for NB-IoT, with near cells significantly correlated even at large distances. As anticipated above, this insight can be an important guideline toward the optimization of NB-IoT deployments on top of existing cellular infrastructures, and it could be considered in the definition of schemes for efficient (de-)activation of NB-IoT cells in specific eNBs.

D. Indoor and deep indoor additional losses

We now complement the above analyses on PL outdoor modeling, and provide initial insights on the additional losses due to indoor device placement. In particular, we leverage our indoor campaigns and split them in three scenarios:

Indoor @ *Deep* level (DI), including campaigns where the device was placed in indoor locations below the street level, i.e., in office buildings with no windows;
Indoor @ *Low* level (InL), including campaigns where the device was placed in indoor locations at street level, i.e., in office buildings with windows;
Indoor @ *High* level (InH), including campaigns where the device was placed in indoor locations from 1^{st} to 5^{th} floor, i.e., in office or residential buildings with windows.

For each scenario, we evaluate the deviation between $\overline{\text{PL}}$, as estimated by outdoor models, and real PL values. The deviation indicates the loss to be added to outdoor estimates when DI, InL, and InH deployments are considered. For the outdoor models, we use average values for and ; the indoor measurements are static collections, that thus contain limited fading variations. Given a location, we average all the measurements from a cell and provide a unique PL value.

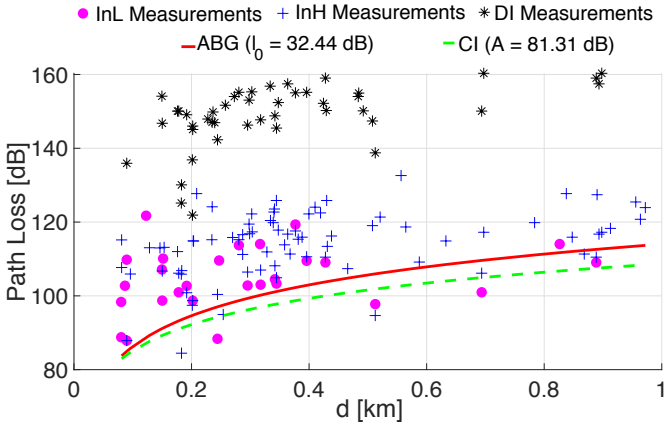

Fig. 14: Difference between PL outdoor estimates given by ABG (red line) and CI (green dashed line) models and indoor measurements, as a function of distance for several cells (InL: magenta dots, InH: blue crosses, DI: black stars).

Figure 14 shows how DI, InL, and InH measurements distribute over distance. For comparison, we report $\overline{\text{PL}}$ estimates over the same set of distances, for both models. Note that the figure reports measurements from different cells. As observed throughout the paper, multiple cells are usually detected in the same location, leading to different distance points in Fig. 14.

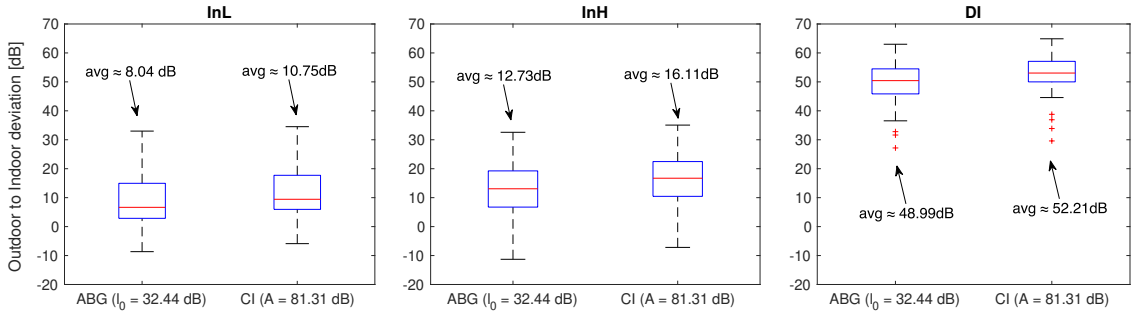

Fig. 15: Statistics and average value of the difference between PL outdoor estimates given by ABG and CI models and InL (left), InH (middle), and DI (right) measurements.

We observe that InL and InH measurements slightly increase the PL compared to outdoor estimates. A few measurements points result even overestimated by the models. A significant PL underestimation is instead observed for DI, which emphasizes the strong impact on signal attenuation.

We quantify these findings in Fig. 15, where the deviations between outdoor estimates and indoor measurements are reported in boxplots, as a function of the adopted model and for the three indoor scenarios. As regards InL (left), we see that such a deployment results in an average additional loss of about 8 dB and 11 dB for ABG and CI estimates, respectively. The average loss increases to about 13 dB and 16 dB for InH situations (middle). The difference between InL and InH could be due to a stronger impact of ground reflections in the former case that could result in constructive interference and thus higher received signal power. Moving on DI (right), we see a significant PL increase, resulting in average values of about 49 dB and 52 dB for ABG and CI, respectively.

Compared to the values adopted in NB-IoT simulation-based studies (10 dB, 20 dB, and 30 dB, see §II), we see that the first two values roughly approximate the empirical observations in InL and InH. However, at a first glance, the value of 30 dB seems to significantly underestimate DI losses.

On this aspect, we underline two experimental limitations which we plan to overcome in the next-future via further measurement campaigns: a) the set of indoor locations we tested is rather limited, and b) for DI, we have collected data for two extreme enclosed locations (i.e., two floors under the ground level, with iron doors and no windows). Hence, our empirical findings are, in their current status, not generalizable and cannot be validated statistically. Still, we believe they provide an effective guideline for the application of the proposed ABG and CI models in simulating NB-IoT indoor deployments, while highlighting the need for more extensive investigations.

VI. Conclusion

In this paper, we present the first empirical characterization of NB-IoT PL in an urban scenario. By exploiting a large scale measurement campaign in Oslo, we provide statistically extended ABG and CI models for PL average term, along with shadowing distribution and correlation over distance. Moreover, we analyze inter-site shadowing correlation and give numerical indications on the additional losses to consider when using the models for simulating outdoor-to-indoor propagation. The models enable realistic simulations of NB-IoT propagation in Oslo-like multi-cell urban deployments, improving the PL estimation accuracy given by existing models adopted in NB-IoT works, which are not derived from NB-IoT measurements. Future work will include the collection and analysis of further measurements, in both outdoor scenarios (i.e., other cities and suburban areas) and indoor locations, aiming at model validation and extension.

VII. Acknowledgment

This work is partly funded by the EU H2020 research and innovation programme, grant agreement No. 815178 (5GENESIS).

References

[1] U. Raza, P. Kulkarni, and M. Sooriyabandara, "Low Power Wide Area Networks: An Overview," *IEEE Commun. Surveys Tuts.*, vol. 19, no. 2, pp. 855–873, 2017.

[2] O. Liberg *et al.*, *Cellular Internet of Things: From Massive Deployments to Critical 5G Applications, 2nd Edition*. Academic Press, 2020.

[3] Y.-P. E. Wang *et al.*, "A Primer on 3GPP Narrowband Internet of Things," *IEEE Commun. Mag.*, vol. 55, no. 3, pp. 117–123, 2017.

[4] J. Xu *et al.*, "Narrowband Internet of Things: Evolutions, Technologies, and Open Issues," *IEEE Internet Things J.*, vol. 5, no. 3, pp. 1449–1462, 2017.

[5] GSMA, "NB-IoT Deployment Guide to Basic Feature Set Requirements," https://www.gsma.com/iot/wp-content/uploads/2019/07/201906-GSMA-NB-IoT-Deployment-Guide-v3.pdf, Accessed: Nov. 2020.

[6] T. S. Rappaport *et al.*, *Wireless Communications: Principles and Practice*. Prentice Hall PTR New Jersey, 1996, vol. 2.

[7] N. Jaldén *et al.*, "Inter- and Intrasite Correlations of Large-Scale Parameters from Macrocellular Measurements at 1800 MHz," *EURASIP Journal on Wireless Communications and Networking*, vol. 2007, pp. 1–12, 2007.

[8] M. Zhu, F. Tufvesson, and J. Medbo, "Correlation Properties of Large Scale Parameters From 2.66 GHz Multi-Site Macro Cell Measurements," in *Vehicular Technology Conference (VTC-Spring'11)*. IEEE, 2011, pp. 1–5.

[9] P. Heino *et al.*, "D5.3: Winner+ final channel models," *V1.0*, 2010.

[10] S. Sun *et al.*, "Propagation Path Loss Models for 5G Urban Micro- and Macro-Cellular Scenarios," in *Vehicular Technology Conference (VTC-Spring'16)*. IEEE, 2016, pp. 1–6.

[11] K. Haneda *et al.*, "5G 3GPP-like Channel Models for Outdoor Urban Microcellular and Macrocellular Environments," in *Vehicular Technology Conference (VTC-Spring'16)*. IEEE, 2016, pp. 1–7.

[12] V. Erceg *et al.*, "An Empirically Based Path Loss Model for Wireless Channels in Suburban Environments," *IEEE J. Sel. Areas Commun.*, vol. 17, no. 7, pp. 1205–1211, 1999.

[13] H. Linka *et al.*, "Path Loss Models for Low-Power Wide-Area Networks: Experimental Results using LoRa," 2018.

[14] K. Q. Abdelfadeel, Y. Samarawickrama, and V. Cionca, "How To Conduct LoRAWAN Site Surveys," in *Int'l Conf. on Wireless and Mobile Computing, Networking and Communications (WiMob'19)*. IEEE, 2019, pp. 133–138.

[15] R. El Chall, S. Lahoud, and M. El Helou, "LoRaWAN Network: Radio Propagation Models and Performance Evaluation in Various Environments in Lebanon," *IEEE Internet Things J.*, vol. 6, no. 2, pp. 2366–2378, 2019.
[16] N. Mangalvedhe, R. Ratasuk, and A. Ghosh, "NB-IoT Deployment Study for Low Power Wide Area Cellular IoT," in *Annual Int'l Symp. on Personal, Indoor, and Mobile Radio Communications (PIMRC'16)*. IEEE, 2016, pp. 1–6.
[17] A. E. Mostafa, Y. Zhou, and V. W. Wong, "Connectivity Maximization for Narrowband IoT Systems with NOMA," in *Int'l Conf. on Communications (ICC'17)*. IEEE, 2017, pp. 1–6.
[18] ——, "Connection Density Maximization of Narrowband IoT Systems with NOMA," *IEEE Trans. Wireless Commun.*, vol. 18, no. 10, pp. 4708–4722, 2019.
[19] W. Hou *et al.*, "Interference-Aware Subcarrier Allocation for Massive Machine-Type Communication in 5G-Enabled Internet of Things," *Sensors*, vol. 19, no. 20, p. 4530, 2019.
[20] S. Mishra, L. Salaun, and C. S. Chen, "Maximizing connection density in nb-iot networks with noma," in *Vehicular Technology Conference (VTC-Spring'20)*, 2020.
[21] H. Malik *et al.*, "Radio resource management scheme in nb-iot systems," *IEEE Access*, vol. 6, pp. 15 051–15 064, 2018.
[22] J.-M. Liang *et al.*, "Energy-efficient uplink resource units scheduling for ultra-reliable communications in nb-iot networks," *Wireless Communications and Mobile Computing*, vol. 2018, 2018.
[23] Z. Mlika and S. Cherkaoui, "Massive Access in Beyond 5G IoT Networks with NOMA: NP-hardness, Competitiveness and Learning," *arXiv preprint arXiv:2002.07957*, 2020.
[24] A. Ikpehai *et al.*, "Low-Power Wide Area Network Technologies for Internet-of-Things: A Comparative Review," *IEEE Internet Things J.*, vol. 6, no. 2, pp. 2225–2240, 2018.
[25] L. Bao *et al.*, "Coverage analysis on nb-iot and lora in power wireless private network," *Procedia Computer Science*, vol. 131, pp. 1032–1038, 2018.
[26] M. Lauridsen *et al.*, "Coverage Comparison of GPRS, NB-IoT, LoRa, and SigFox in a 7800 km^2 Area," in *Vehicular Technology Conference (VTC-Spring'17)*. IEEE, 2017, pp. 1–5.
[27] B. Vejlgaard *et al.*, "Coverage and Capacity Analysis of SigFox, LoRa, GPRS, and NB-IoT," in *Vehicular Technology Conference (VTC-Spring'17)*. IEEE, 2017, pp. 1–5.
[28] K. Kousias *et al.*, "Coverage and Deployment Analysis of Narrowband Internet of Things in the Wild," *IEEE Commun. Mag.*, vol. 58, no. 9, pp. 39–45, 2020.
[29] https://mosaic-simulamet.com/nbiotcoverage, Accessed: Nov. 2020.
[30] G. R. MacCartney *et al.*, "Path Loss Models for 5G Millimeter Wave Propagation Channels in Urban Microcells," in *Global Communications Conference (GLOBECOM'13)*. IEEE, 2013, pp. 3948–3953.
[31] J. B. Andersen, T. S. Rappaport, and S. Yoshida, "Propagation Measurements and Models for Wireless Communications Channels," *IEEE Commun. Mag.*, vol. 33, no. 1, pp. 42–49, 1995.
[32] M. Gudmundson, "Correlation model for shadow fading in mobile radio systems," *Electronics Letters*, vol. 27, no. 23, pp. 2145–2146, 1991.
[33] V. Graziano, "Propagation Correlations at 900 MHz," *IEEE Trans. Veh. Technol.*, vol. 27, no. 4, pp. 182–189, 1978.
[34] K. Zayana and B. Guisnet, "Measurements and modelisation of shadowing cross-correlations between two base-stations," in *Int'l Conf. on Universal Personal Communications (ICUPC'98)*, vol. 1. IEEE, 1998, pp. 101–105.
[35] J. Weitzen and T. J. Lowe, "Measurement of angular and distance correlation properties of log-normal shadowing at 1900 mhz and its application to design of pcs systems," *IEEE Trans. Veh. Technol.*, vol. 51, no. 2, pp. 265–273, 2002.
[36] N. Jaldén *et al.*, "Correlation Properties of Large Scale Fading based on Indoor Measurements," in *Wireless Communications and Networking Conference (WCNC'07)*. IEEE, 2007, pp. 1894–1899.
[37] B. Martinez *et al.*, "Exploring the Performance Boundaries of NB-IoT," *IEEE Internet Things J.*, vol. 6, no. 3, pp. 5702–5712, 2019.
[38] ITU-R, "Guidelines for Evaluation of Radio Interface Technologies for IMT-Advanced," M Series, Mobile, radiodetermination, amateur and related satellites services, https://www.itu.int/dms_pub/itu-r/opb/rep/R-REP-M.2135-1-2009-PDF-E.pdf, Accessed: Nov. 2020.
[39] 3GPP, "5G; Study on channel model for frequencies from 0.5 to 100 GHz (v. 14.1.1 Release 14)," TS 38.901, https://www.etsi.org/deliver/etsi_tr/138900_138999/138901/14.01.01_60/tr_138901v140101p.pdf, Accessed: Nov. 2020.
[40] ——, "Universal Mobile Telecommunications System (UMTS); Selection procedures for the choice of radio transmission technologies of the UMTS (UMTS 30.03 v. 3.2.0)," UMTS 30.03, https://www.etsi.org/deliver/etsi_tr/101100_101199/101112/03.02.00_60/tr_101112v030200p.pdf, Accessed: Nov. 2020.
[41] ——, "Cellular System Support for Ultra Low Complexity and Low Throughput Internet of Things," TR 45.820, https://portal.3gpp.org/desktopmodules/Specifications/SpecificationDetails.aspx?specificationId=2719, Accessed: Nov. 2020.
[42] A. R. Mishra, *Advanced Cellular Network Planning and Optimisation: 2G/2.5 G/3G...evolution to 4G*. John Wiley & Sons, 2007.
[43] 3GPP, "Lte; evolved universal terrestrial radio access (e-utra); base station (bs) radio transmission and reception," TS 36.104, https://www.etsi.org/deliver/etsi_ts/136100_136199/136104/14.03.00_60/ts_136104v140300p.pdf, accessed: May 2020.
[44] K. M. Malarski *et al.*, "Investigation of Deep Indoor NB-IoT Propagation Attenuation," in *Vehicular Technology Conference (VTC-Fall'19)*. IEEE, 2019, pp. 1–5.
[45] J. Thrane *et al.*, "Experimental Evaluation of Empirical NB-IoT Propagation Modelling in a Deep-Indoor Scenario," *arXiv preprint arXiv:2006.00880*, 2020.
[46] K. M. Malarski *et al.*, "Understanding sub-GHz Signal Behaviour in Deep-Indoor Scenarios," *IEEE Internet Things J.*, 2020.
[47] G. Caso *et al.*, "NB-IoT Random Access: Data-driven Analysis and ML-based Enhancements," *IEEE Internet Things J.*, 2021.
[48] https://mosaic-simulamet.com/nbiot-randomaccess, accessed: May 2020.
[49] R. W. Sinnott, "Virtues of the haversine," *Sky Telesc.*, vol. 68, p. 159, 1984.
[50] W. C. Lee, "Estimate of Local Average Power of a Mobile Radio Signal," *IEEE Trans. Veh. Technol.*, vol. 34, no. 1, pp. 22–27, 1985.
[51] H. W. Lilliefors, "On the kolmogorov-smirnov test for normality with mean and variance unknown," *Journal of the American statistical Association*, vol. 62, no. 318, pp. 399–402, 1967.
[52] P. Jörke *et al.*, "Urban Channel Models for Smart City IoT-Networks based on Empirical Measurements of LoRa-links at 433 and 868 MHz," in *Annual Int'l Symp. on Personal, Indoor, and Mobile Radio Communications (PIMRC'17)*. IEEE, 2017, pp. 1–6.

BIOGRAPHIES

Giuseppe Caso [M] is a Postdoctoral Fellow with the Mobile Systems and Analytics (MOSAIC) Department at Simula Metropolitan (SimulaMet). In 2016, he received the Ph.D. degree from Sapienza University of Rome, where he was a Postdoctoral Fellow until 2018. From 2012 to 2018, he has held visiting positions at Leibniz University of Hannover, King's College London, Technical University of Berlin, and Karlstad University. His research interests include cognitive communications, distributed learning, IoT technologies, and WiFi/UWB positioning systems.

Özgü Alay [M] received the B.Sc. and M.Sc. degrees in Electrical and Electronic Engineering from Middle East Technical University, Turkey, and Ph.D. degree in Electrical and Computer Engineering at Tandon School of Engineering at New York University. She is currently an Associate Professor in University of Oslo, Norway and Head of Department at Mobile Systems and Analytics (MOSAIC) of Simula Metropolitan, Norway. Her research interests lie in the areas of 5G networks, Internet of Things, drone communications, mobile multimedia systems, and multipath protocols. She is author of more than 70 peer-reviewed IEEE and ACM publications and she actively serves on technical boards of major conferences and journals.